

Electronic Supplementary Information

**Role of topological scale in the differential fouling of  
*Pseudomonas aeruginosa* and *Staphylococcus aureus*  
bacterial cells on wrinkled gold-coated polystyrene surfaces**

*Duy H. K. Nguyen,<sup>†</sup> Vy T. H. Pham,<sup>†</sup> Vi Khanh Truong,<sup>†</sup> Igor Sbarski,<sup>‡</sup> James Wang,<sup>‡</sup> Armandas Balcytis,<sup>†</sup> Saulius Juodkazis,<sup>†</sup> David E. Mainwaring,<sup>†</sup> Russell J. Crawford,<sup>§</sup> and Elena P. Ivanova<sup>\*,†</sup>*

<sup>†</sup>School of Science, Faculty of Science, Engineering and Technology, Swinburne University of Technology, Hawthorn VIC 3122, Australia

<sup>‡</sup>School of Engineering, Faculty of Science, Engineering and Technology, Swinburne University of Technology, Hawthorn VIC 3122, Australia

<sup>§</sup>School of Science, College of Science, Engineering and Health, RMIT University, Melbourne VIC 3001, Australia

**Corresponding Author**

\*Email: [eivanova@swin.edu.au](mailto:eivanova@swin.edu.au). Tel.: +61 3 9214 5137

## **Supplementary experimental details**

**Glass transition temperature.** The effect of the gold coating on the glass transition temperature ( $T_g$ ) was assessed by using the Dynamic Mechanical Analyzer 2980 (TA Instruments, USA). The  $T_g$  was determined by the Tan Delta peak, which allowed a comparison to be made between the coated and non-coated samples.

**Fourier transform infrared spectroscopy (FTIR).** Infrared spectra were obtained in the ATR mode at the Australian Synchrotron Infrared Microspectroscopy beamline using a Bruker Hyperion 2000 Fourier transform infrared (FTIR) microscope (Ettlingen, Germany), equipped with a 36 $\times$  (NA 0.5) reflecting objective and condenser and a narrow-band mercury cadmium telluride detector. Low-resolution spectra were first obtained from an area of 400  $\mu\text{m} \times 600 \mu\text{m}$  before taking high-resolution spectra in 100  $\mu\text{m} \times 300 \mu\text{m}$  using an accumulation of 16 scans. The chemical mapping was conducted based on the selected peak area in the high-resolution spectra. Asymmetric stretching vibrations of methylene groups  $=\text{CH}_2$  was employed to shown the stability of chemical bonding on the A.R. polystyrene sample after heat treatment.

**Wrinkle pattern characteristics.** Wrinkled patterns, as a consequence of surface instability, comprises two characteristic parameters: amplitude and wavelength. Both can be expressed in a similar manner t waves, where they represent height and frequency respectively (Table 2). Since the undulation was isotropic, the wrinkle topology appeared to be hierarchical and organized in a way that small wrinkles formed on top of the larger wrinkles. The amplitude of each specific wrinkle type was assessed using the surface line profile from atomic force micrographs AFM (Fig. 1), whereas, the Fast Fourier Transform (FFT) reveals the spatial periodicity of pattern, was employed on scanning electron micrographs (SEM) to estimate the spacing (wavelength) (Fig. 2).”

**X-ray photoelectron spectroscopy (XPS).** During analysis, the samples were flooded with low-energy electrons to counteract any surface charging that may take place. The hydrocarbon component of the C 1s peak (binding energy 284.8 eV) was used as a reference for charge correction. The Shirley algorithm was used to measure the background core level spectra and chemically distinct species in the high-resolution regions of the spectra were resolved using synthetic Gaussian–Lorentzian components after the background was removed (using the Thermo Scientific™ Avantage Data System).

**Wettability and air detection.** Time lapsed imaging of a water droplet on the substrate surfaces was conducted in a sealed humid environment for 3 h, in which samples with a water droplet was surrounded by wetted tissues and covered inside a transparent box. The evaporation of the water droplet at the liquid-air interface was minimized and the wetting procedure was only based on the stability of the trapped air within the nanostructures.

## **Supplementary Results and Discussion**

### **Formation of wrinkle patterned polystyrene surfaces**

In the gold-polystyrene bilayer system, the compressive stresses were triggered at the interface due to the mismatch between a soft foundation layer (polystyrene) and a hard skin (gold). The external stimulus required for the formation of wrinkles needed to be above the glass transition temperature ( $T_g$ ) of the substrate in order to cause the polystyrene to shrink.<sup>1</sup> Since the wrinkle formation is dependent on  $T_g$ , the thermal property of the commercial polystyrene sample needed to be compared under both the non-coating and coating conditions. The  $T_g$  was clarified by the Tan Delta peak method using the dynamic mechanical analysis described in Supplementary section. It was illustrated that the  $T_g$  was identical for both conditions at 106°C, which is close to the literature value of polystyrene (107 °C) (Fig. S1).<sup>2</sup> In addition, FTIR was used to confirm the origin of the commercial polystyrene samples (Table

S-1 and Fig. S-1). In this work, the stiffness mismatch was leveraged by the presence of two different gold coating thicknesses at 2.2 nm and 11 nm in order to fabricate two distinctive wrinkled surfaces. In order to achieve these two-dimensional wrinkled surfaces, gold-coated polystyrene samples were shrunk at 130°C for 30 minutes, without any restraints, in biaxial directions.

**Stability of air entrapment.** The air retained inside the wrinkled surfaces remained stable for at least 3 hours as evidenced by the time-lapse imaging illustrated in Fig. 3. The wrinkle structures contributed to the high measured water contact angle in the W2 (123.8°) and W11 (130.0°) samples compared to that of 53.6° measured on the flat control samples. Furthermore, water droplets present on the wrinkled surfaces followed the Cassie-Baxter model in that the water contacted a surface comprised of both substrate surface and entrapped air. In order to further examine the stability of these interfaces, a closed system containing additional humidity was designed to minimize the likelihood of water evaporation at the gas-liquid. The shape and size of an 8.0  $\mu$ L water droplet remained intact over 3 hours, as shown in Fig. S-4.

**Table S-1.** IR absorption bands and their assignments of as-received polystyrene surfaces.

| frequency (cm <sup>-1</sup> ) | band assignment   |
|-------------------------------|---|
| 1002 – 1036                   | aromatic in-plane C–H bending   |
| 1432 – 1474                   | aromatic C–C stretching vibrations                                    |
| 1479 – 1513                   | aromatic C–C stretching vibrations                                    |
| 1584 – 1618                   | aromatic C–C stretching vibrations                                    |
| 2826 – 2867                   | symmetric stretching vibrations of methylene groups =CH <sub>2</sub>  |
| 2880 – 2975                   | asymmetric stretching vibrations of methylene groups =CH <sub>2</sub> |
| 3019 – 3053                   | aromatic =C–H stretching  |

**Table S-2.** XPS elemental analysis<sup>a</sup> of Au, C, O and N on planar polystyrene and wrinkled surfaces covered with a 2.2 nm (W2) and 11 nm (W11) thin gold coating.

| Sample | Au         | C          | O          | N         |
|--------|------------|------------|------------|-----------|
| PS     | 0.0 ± 0.0  | 76.9 ± 9.9 | 19.7 ± 4.7 | 3.2 ± 0.9 |
| W2     | 17.4 ± 1.5 | 60.1 ± 5.4 | 17.1 ± 1.4 | 5.4 ± 2.6 |
| W11    | 49.1 ± 2.2 | 37.8 ± 7.9 | 10.8 ± 2.4 | 2.4 ± 0.9 |

<sup>a</sup> Surface compositions from XPS analysis as atomic percentage (at. %)

**Table S-3.** Water contact angle and surface roughness ( $S_a$ ) for polystyrene (PS) and planar surfaces covered with a 2.2 nm (F2) and 11 nm (F11) thin gold coating.

|                                   | PS         | F2         | F11        |
|-----------------------------------|------------|------------|------------|
| Water contact angle, $\theta$ (°) | 53.6 ± 4.0 | 73.7 ± 7.8 | 94.4 ± 2.2 |
| $S_a$ (nm)                        | 2.4 ± 0.6  | 2.9 ± 0.5  | 4.7 ± 0.7  |

**Table S-4.** Bacterial viability (damage) of attached bacteria shown in Fig. 5 as determined by LIVE/DEAD BacLight Bacterial Viability Kit.

| <i>P. aeruginosa</i> | Live cell (%) | Damaged cell (%) |
|----------------------|---------------|------------------|
| PS                   | 86.5          | 13.5             |
| F2                   | 97            | 3                |
| F11                  | 80.9          | 19.1             |
| W2                   | 83.3          | 16.7             |
| W11                  | 82.4          | 17.6             |
| <i>S. aureus</i>     | Live cell (%) | Damaged cell (%) |
| PS                   | 77.1          | 22.9             |
| F2                   | 75.5          | 24.5             |
| F11                  | 81.3          | 18.7             |
| W2                   | 94.3          | 5.7              |
| W11                  | 95.5          | 4.5              |

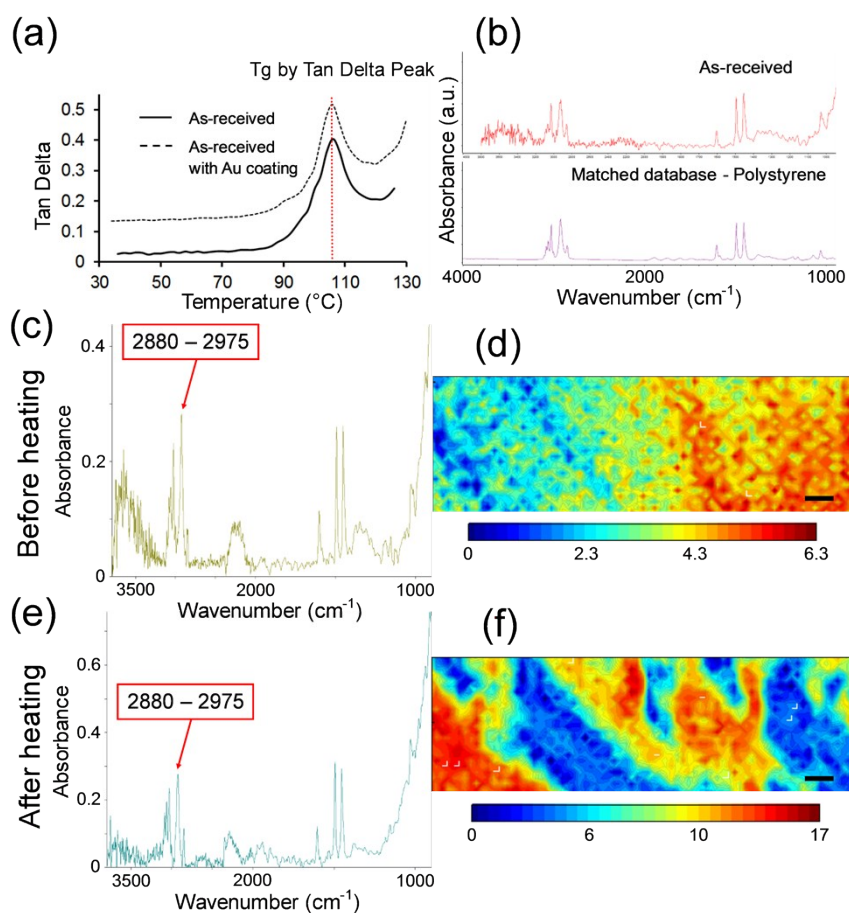


**Figure S-1.** Synchrotron Radiation Fourier Transform Infrared Spectroscopic analysis of as – received polystyrene samples before and after heat treatment. (a) Glass transition temperature determined by the Tan Delta Peak method of the A.R. commercial polystyrene substrate showed no difference in composition with and without the gold coating. (b) Comparative spectra of the as-received polystyrene sample and that of polystyrene IR database. Spectra comparison and chemical mapping for asymmetric stretching vibrations of  $=CH_2$  of the as-received polystyrene plastic sample (c, d) before and (e, f) after heat treatment (130°C) (refer to Table S1). Scale bars in chemical maps are 20  $\mu m$ . The discrepancy in mapping is due to the inhomogeneity of the polystyrene surface after shrinking.

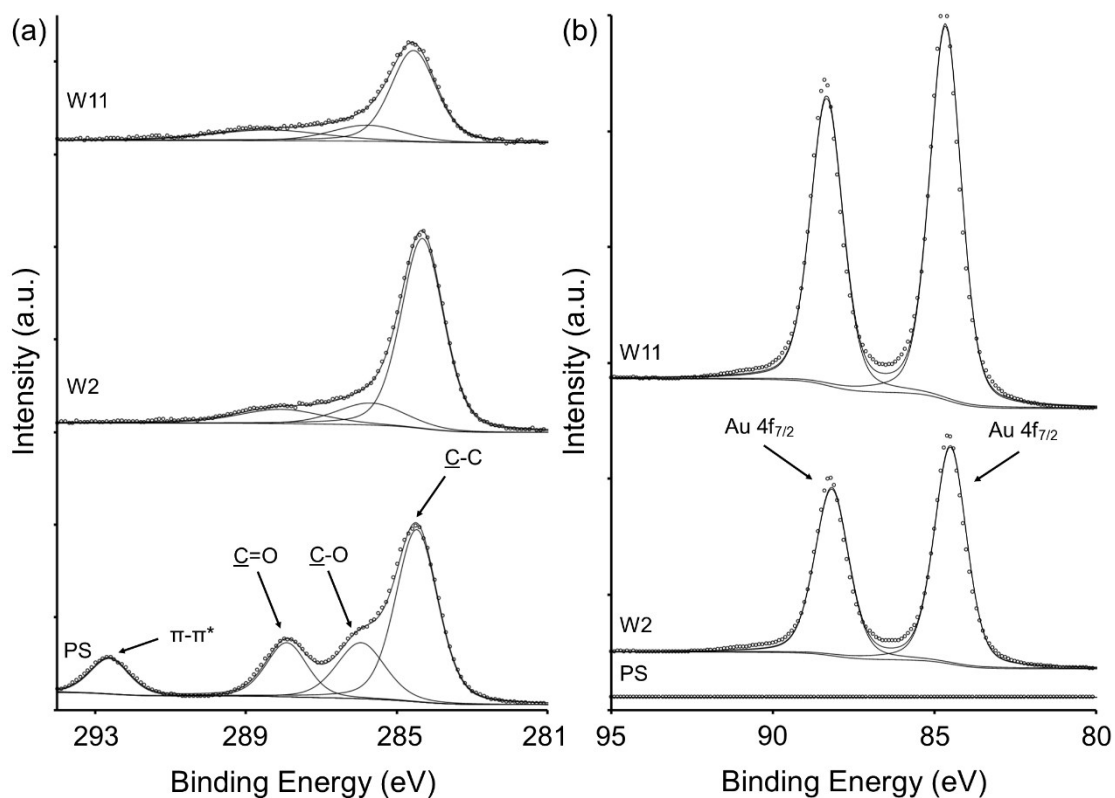


**Figure S-2.** The elemental composition, examined by XPS, of the planar (PS) and wrinkled surfaces (W2 and W11). (a) High-resolution spectra of carbon (C 1s) confirmed the presence of adventitious carbon contamination (C=O and C-O) and characteristic aromatic ( $\pi-\pi^*$ ) with strong C-C bonding of polystyrene. (b) High-resolution spectra of gold (Au 4f) appeared as an increasing surface coverage by gold, which caused a reduction in the intensity of the C1s peaks.



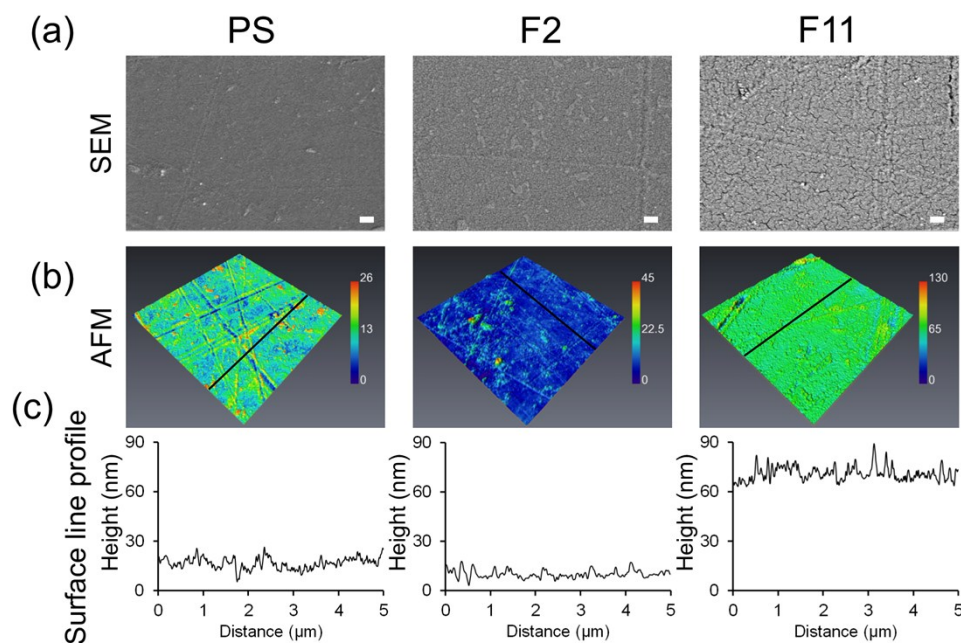


**Figure S-3.** Surface morphology of the planar surfaces including polystyrene (PS), polystyrene covered with a 2.2 nm (F2) and 11 nm (F11) thin gold coating visualized using (a) SEM and (b) AFM. AFM micrographs were taken over a scanning area of  $5\ \mu\text{m} \times 5\ \mu\text{m}$ , with (c) the corresponding surface line profile representing the roughness. Colour scale bars in AFM micrographs are in nm. Scale bars in SEM micrographs are 200 nm.

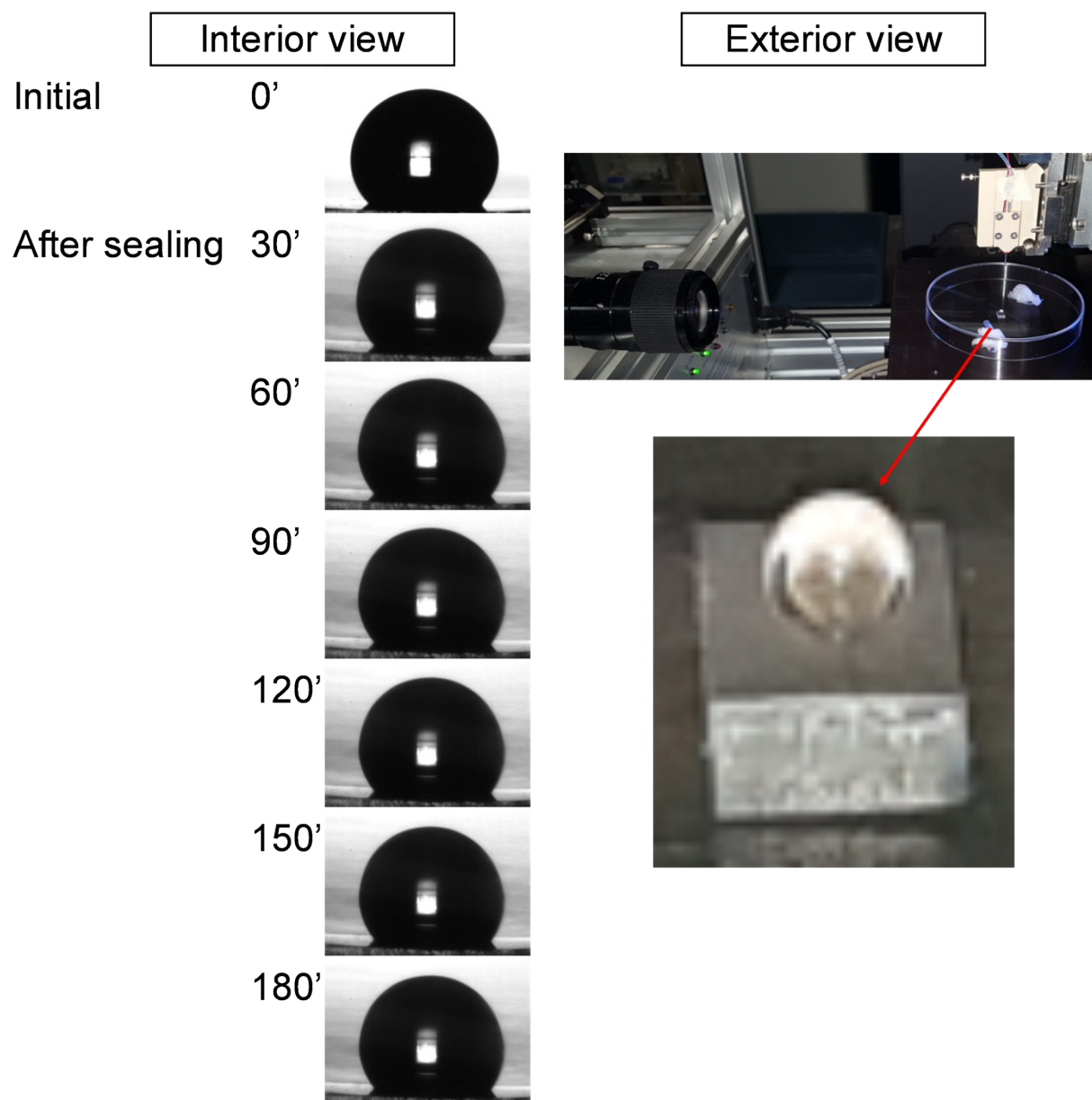


**Figure S-4.** Time lapsed imaging of a water droplet on the surface of wrinkled polystyrene covered with an 11 nm (W11) thin gold coating in a closed humid environment. The sealed environment with high moisture minimized the evaporation procedure of water droplet at the liquid-air interface. The droplet remained constant in size for at least 3 hours.

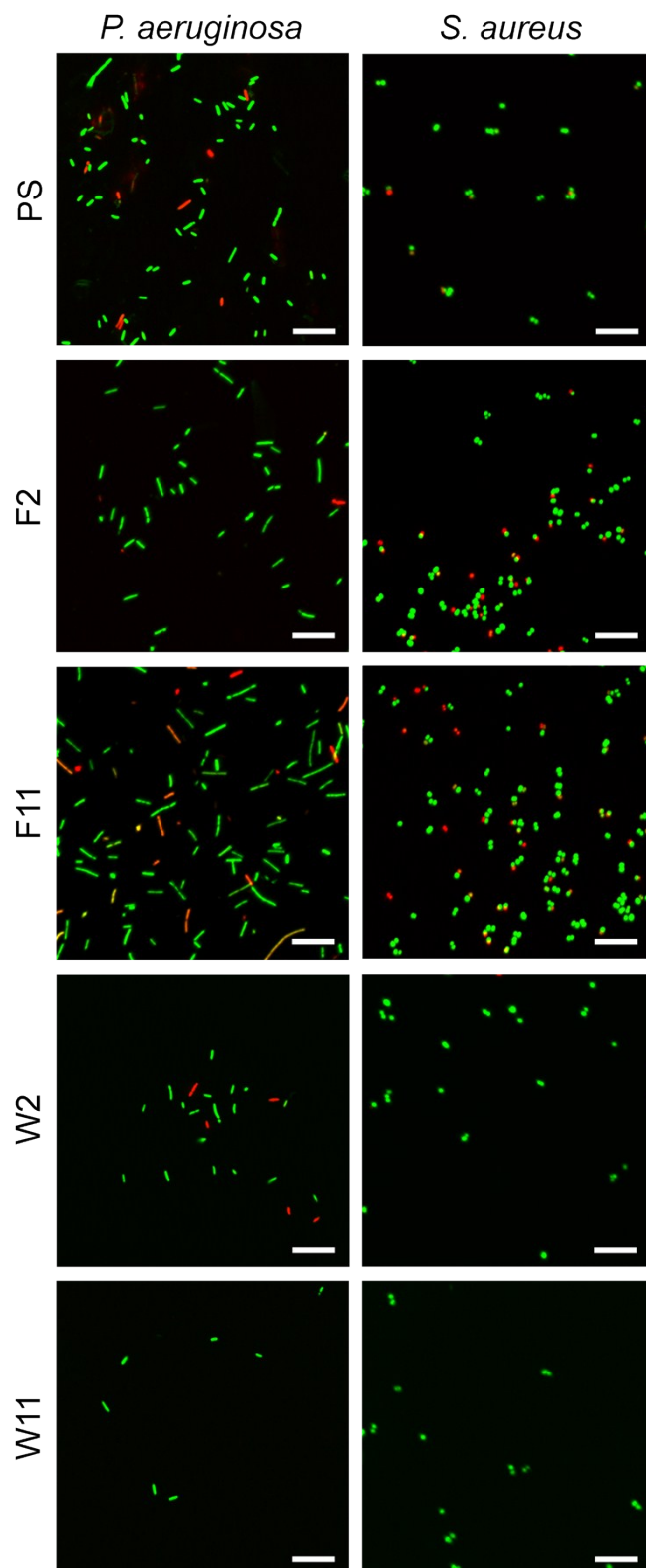


**Figure S-5.** Enhanced CLSM micrographs of *P. aeruginosa* and *S. aureus* bacterial cells. Live cells are stained green; damaged cells are stained red. Scale bars are 10  $\mu\text{m}$ .

## Reference

1. J. Rodríguez-Hernández, *Prog. Polym. Sci.*, 2015, **42**, 1-41.
2. J. Rieger, *J. Therm. Anal.*, 1996, **46**, 965-972.